Robust Scattered Fields from Adiabatically Driven Targets around Exceptional Points

Lucas J. Fernández-Alcázar,[1,*] Huanan Li,[1,2,*] Fred Ellis,[1] Andrea Alú,[2] and Tsampikos Kottos[1]
[1]Wave Transport in Complex Systems Lab, Department of Physics, Wesleyan University, Middletown, Connecticut 06459, USA
[2]Photonics Initiative, Advanced Science Research Center, CUNY, New York 10031, USA

(Received 21 December 2019; accepted 16 March 2020; published 2 April 2020)

Scattering processes are typically sensitive to the incident wave properties and to interference effects generated via wave-matter interactions with the target. We challenge this general belief in the case of targets that undergo time-periodic modulations encircling quasiadiabatically an exceptional point in a given parameter space. When the scattering dwell time is above a critical value τ_c, the scattered field is surprisingly insensitive to the properties of the incoming wave and local operational details of the driving. Instead, it reaches a fixed point attractor that can be controlled by the direction of the driving cycle. For dwell times below τ_c, the unusual robustness is abruptly suppressed. Such protocols may become useful tools in control engineering, including the management of thermal and quantum fluctuations.

DOI: 10.1103/PhysRevLett.124.133905

Introduction.—Wave scattering from naturally occurring or engineered media carries information about the properties (e.g., shape, internal constitution) of the scattering object itself, convoluted with the impinging signal. A challenge in modern technology is to manage, amplify, alter, or encrypt this information. The traditional methods used to achieve these goals rely on the manipulation of the constituent properties of the scattering medium and/or on the appropriate preparation of the interrogating wave. Well-known examples include metamaterials and transformation optics [1–10], and the enhancement of absorption [11–16] or the improvement of transmission through complex media [17,18] by wavefront optimization. The advent of non-Hermitian wave physics [19–23] has opened alternative avenues for the manipulation of the scattered fields. Representative examples include the phenomena of unidirectional invisibility [24–26], asymmetric transport [27–30], and $\mathcal{PT}$-symmetric lasers [31,32]. When combined with the manipulation of time degrees of freedom (e.g., via periodic time modulation of system parameters) non-Hermitian physics leads to new opportunities, such as chiral adiabatic state-flip [33–37], reconfigurable perfect absorbers [38–40], bypass of Chu's limit [41], etc. While most of these achievements have been implemented in photonics, other areas like atomic and quantum systems [42–44], optomechanics [35,45,46], acoustics [25,47], and electronics [48] have also benefited from these developments. In all these cases, the scattered fields demonstrate complex interference patterns, which are very sensitive to the incident wave properties and to interferences generated due to intricate wave-matter interactions occurring when the incident signal engages the target.

In this Letter, we propose to manage the scattered fields via a carefully chosen quasiadiabatic modulation of the parameters of the target, such that their variation forms a closed path (loop) around an exceptional point (EP) in a two-parameter space. We will show that when the dwell time of the scattering process exceeds a critical value, the scattered field becomes insensitive to local details of the parametric path and to the specific features of the incident wave. The overall response only depends on the direction (clockwise versus counterclockwise) of the closed path. The eigenvectors of the scattering matrix play the role of "fixed-point attractors" in the dynamical scattering process. This exotic scattering response is analyzed theoretically using coupled mode theory and its validity is confirmed using a realistic electronic circuit setup.

Coupled mode theory modeling.—We consider a system of two coupled modes $n = 1, 2$ with periodic, time-modulated frequencies $\epsilon_1 = \epsilon(t) = \epsilon(t + 2\pi/\Omega)$ and $\epsilon_2(t) = -\epsilon(t)$, and corresponding decay and amplification rates $\gamma_1 = -\gamma/2$ and $\gamma_2 = \gamma/2$. The coupling $\kappa(t) = \kappa(t + 2\pi/\Omega)$ between the two modes is also time dependent with modulation frequency Ω. The dynamics of this system is described by a time-dependent coupled mode theory (CMT)

$$i\frac{d|\Psi(t)\rangle}{dt} = H_0(t)|\Psi(t)\rangle;$$
$$H_0(t) = \begin{pmatrix} \epsilon(t) - \frac{i\gamma}{2} & \kappa(t) \\ \kappa(t) & -\epsilon(t) + \frac{i\gamma}{2} \end{pmatrix}, \quad (1)$$

where $\langle n|\Psi(t)\rangle = \psi_n(t)$ describes the field amplitudes at modes $n = 1, 2$. The evolution of this time-dependent system is described in terms of the instantaneous (i.e., at a fixed time t) eigenvectors $\{|\lambda_l^t\rangle\}$ $(l = 1, 2)$ and eigenvalues $\{\lambda_l^t\}$ of the Hamiltonian H_0. The latter are

$$\lambda^t_{1,2} = \pm\sqrt{\left(\epsilon(t) - \frac{i\gamma}{2}\right)^2 + \kappa(t)^2}, \tag{2}$$

with corresponding instantaneous eigenvectors

$$|\lambda^t_{1,2}\rangle = \frac{1}{\sqrt{N_{1,2}}}\left(\kappa(t), \lambda^t_{1,2} - \epsilon(t) + i\frac{\gamma}{2}\right)^T, \tag{3}$$

where $N_{1,2} = 2\lambda^t_{1,2}[\lambda^t_{1,2} - \epsilon(t) \mp i\gamma/2]$. For fixed parameters (ϵ, κ), Eqs. (2) and (3) indicate that the system Eq. (1) supports exceptional point (EP) spectral degeneracies. These degeneracies occur at $(\epsilon - i\gamma/2)^2 + \kappa^2 = 0$ and are associated with the coalescence of both eigenvalues and eigenvectors. In the example of Eq. (1) we find that a necessary condition to realize an EP is to have $\epsilon = 0$. Under this condition, we have an EP degeneracy when $\kappa = \gamma/2$. It turns out that the quasiadiabatic evolution of any initial preparation under Hamiltonian $H_0(t)$ results in a final state corresponding to one of the two eigenstates Eq. (3), when the parameters $[\epsilon(t), \kappa(t)]$ change quasiadiabatically forming a closed loop around an EP. The dominant eigenvector of this final state is uniquely determined by the handedness of the EP encirclement in the parameter space. This surprising effect has been recently confirmed in microwave and optomechanical systems [34,35]. The phenomenon has been coined *chiral mode switching* and since its confirmation has attracted much attention, with a number of subsequent studies addressing various aspects in the framework of its Hamiltonian evolution [33,36,38–40].

Here we depart from the Hamiltonian framework of chiral mode switching dynamics and address the following question: are there any traces of this chiral physics in the scattering framework, and, if yes, how do they manifest themselves in the scattered signal? Notice that when the system is coupled to leads, new timescales (e.g., the dwell time) emerge that affect (and even alter) the physics associated with the Hamiltonian dynamics of Eq. (1).

Scattering setup.—We proceed by turning the system of Eq. (1) into a scattering target, see Fig. 1(a). We assume a scenario where an incident monochromatic wave $|S^+\rangle = (s^+_1, s^+_2)^T e^{-i\omega t}$ of frequency ω [49] enters the structure from both sides $n = 1, 2$. In the most general case, its components are random variables, i.e., $s^+_l = S^+_l e^{i\phi_l}$ $(l = 1, 2)$ where S^+_l and ϕ_l are random numbers.

The coupled mode equations that describe the scattering process take the form

$$\begin{aligned} i\frac{d|\Psi(t)\rangle}{dt} &= H_{\text{eff}}|\Psi(t)\rangle + iD|S^+(t)\rangle, \\ |S^-(t)\rangle &= -|S^+(t)\rangle + D^T|\Psi(t)\rangle, \end{aligned} \tag{4}$$

where $|\Psi(t)\rangle$ is the field inside the scatterer and $|S^-(t)\rangle = (S^-_1(t), S^-_2(t))^T$ is the outgoing scattered wave evaluated at some position, with components

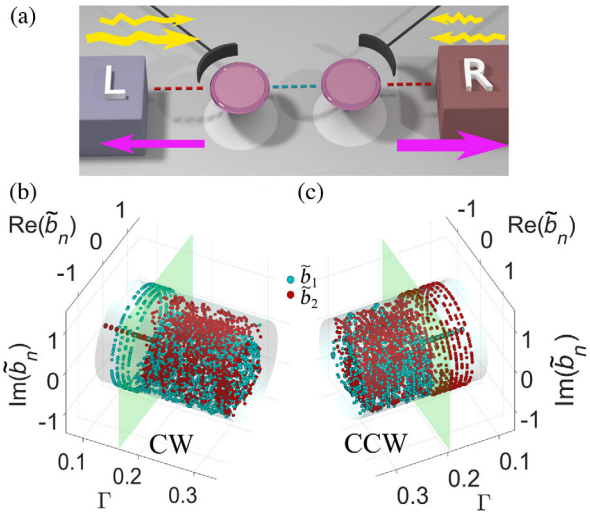

FIG. 1. (a) A scattering setup where an EP degeneracy is adiabatically encircled via the variation of two parameters. Magenta arrows indicate a fixed outgoing scattering field which is independent from incident excitations with random amplitudes and phases (yellow arrows of different width); (b) CW encirclement leads to a scattered field that has a "fixed-point" attractor determined by the mode $|\mu^t_1\rangle$ (i.e., the normalized weight amplitude $\tilde{b}_2 = 0$) for $\Gamma < \Gamma_c$. For $\Gamma > \Gamma_c$, the scattered field is random, i.e., both $\tilde{b}_{1,2}$ depend on the input. (c) The same as in (b) but now for a CCW encirclement. In this case the scattered signal is dominated by $|\mu^t_2\rangle$, i.e., $\tilde{b}_1 = 0$ for $\Gamma < \Gamma_c$. The sharp transition at $\Gamma = \Gamma_c$ is indicated with the transparent green plane. We assumed that $\gamma = 1$ (unit of frequency).

$S^-_l(t) = \int \exp(-i\omega t)\hat{S}_l(\omega)d\omega$. The effective Hamiltonian H_{eff} in Eq. (4) describes the dynamics of the field inside the target and takes into consideration its leakage to the continuum. It has the form

$$H_{\text{eff}} = H_0(t) - (i/2)DD^T; \qquad D = \sqrt{2\Gamma}\hat{I}, \tag{5}$$

where $H_0(t)$ is given by Eq. (1), D describes the coupling of the isolated system to the continuum and $\hat{I}$ is the 2×2 identity operator. For simplicity, we will assume below that $|\Psi(t = 0)\rangle = 0$. Finally, for concreteness, we will use a quasiadiabatic driving scheme $\epsilon_1(t) = -r\sin\varphi(t)$, $\kappa(t) = \kappa_0 + r\cos\varphi(t)$ where $\varphi(t) = \Omega t + \pi/4$ and Ω is the modulation frequency.

It is tempting to argue, based on the similarities between the first Eq. (4) and the time-dependent CMT Eq. (1) that describes the dynamics of an isolated system, that the temporal evolution of the field $|\Psi(t)\rangle$ is the same for the isolated and the scattering setups. There are, however, important differences between these two scenarios. Specifically, in Eq. (4) there is a "noise" term associated with the incident monochromatic wave and an extra "dissipative" term in the effective Hamiltonian that modifies the internal dynamics, see Eq. (5). The latter is described by the coupling operator D, which introduces a

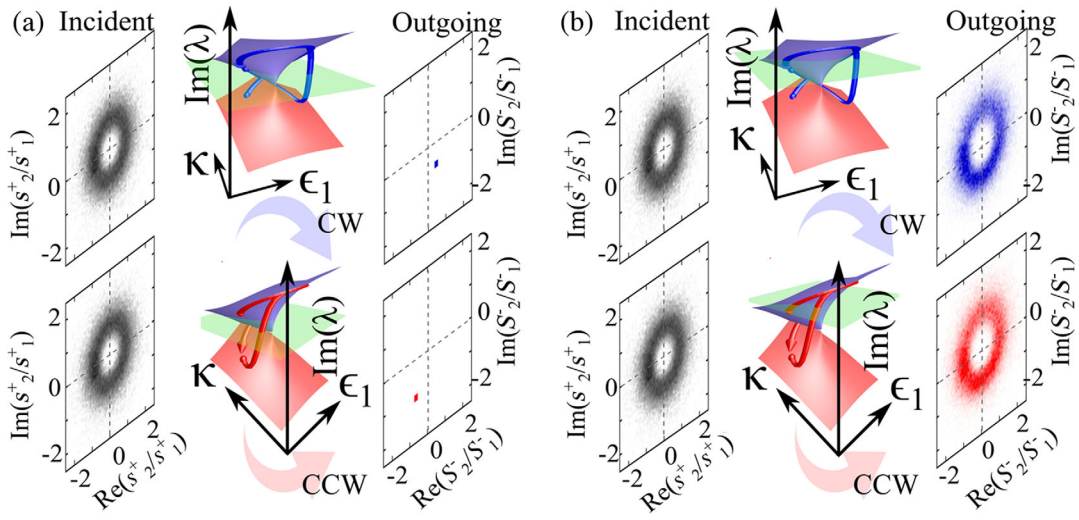

FIG. 2. (a) An ensemble of initial waves $|S^+\rangle$ is sent into a quasiadiabatically modulated linear target when the coupling to the continuum [indicated by the green plane in the $\mathcal{I}m(\lambda)$ axis of the spectrum of H_0] is weak in comparison with the cumulative amplification that the field experiences during one driving cycle. The solid trajectories on the eigenfrequencies surfaces represent the measure $p(t) = [|a_1(t)|^2\lambda_1^t + |a_2(t)|^2\lambda_2^t]/[|a_1(t)|^2 + |a_2(t)|^2]$, which quantifies the relative weight with which each instantaneous eigenvalue and the corresponding eigenvector $|\lambda_{1,2}^t\rangle$ participate in the internal evolution. The weights $a_{1,2}$ are evaluated via the decomposition of the evolved state $|\Psi\rangle$ in the instantaneous basis of H_0. At the end of the CW (CCW) loop around an EP (upper [lower] subfigures) the field inside the scatterer is dominated by only one eigenmode, residing at the blue (red) Riemann surface. This internal dynamics overwhelms the outgoing signal, $|S^-\rangle = (S_1^-, S_2^-)^T$, whose ratio S_2^-/S_1^- reaches a fixed-point attractor (see red and blue points at the outgoing panel). (b) The same as in (a) but for a strong coupling to the continuum. In this case, the outgoing signal is largely influenced by the properties of the incident wave.

new time scale $\tau \sim 1/\Gamma$. It defines the time for which the field dwells inside the target before it decays back into the continuum.

Analysis of scattered fields.—We decompose the outgoing wave $|S^-(t)\rangle$ in terms of the eigenvectors $\{|\mu_l^t\rangle\}$ $(l = 1, 2)$ of the instantaneous scattering matrix S^t as $|S^-(t)\rangle = b_1(t)|\mu_1^t\rangle + b_2(t)|\mu_2^t\rangle$. The relative weights $b_{1,2}(t)$ have been evaluated after an initial transient—typically associated with times t larger than two or three periods of the driving.

The matrix S^t is then derived from Eq. (4), assuming a steady state solution. It takes the form:

$$S^t|\mu^t\rangle = \mu^t|\mu^t\rangle; \quad S^t = -\hat{I} + iD^T G_{\text{eff}}^t D, \quad G_{\text{eff}}^t = \frac{1}{\omega\hat{I} - H_{\text{eff}}^t}, \tag{6}$$

where $H_{\text{eff}}^t = H_{\text{eff}}(t = \text{fixed})$ indicates the instantaneous Hamiltonian Eq. (5) at time t. In our case of $D = \sqrt{2\Gamma}\hat{I}$, eigenvectors of S^t are the same as the eigenvectors of H_0 and do not depend on the incident frequency ω.

Figures 1(b) and 1(c) show the real and imaginary parts of the normalized weights $\tilde{b}_l = b_l/\sqrt{|b_1|^2 + |b_2|^2}$, $(l = 1, 2)$ versus the coupling strength Γ for two counter-encirclements of the EP. For each value of Γ, we generated a number of incident waves with components (s_1^+, s_2^+) having normally (uniformly) distributed random relative amplitudes (phases). We find an abrupt transition occurring above a critical coupling strength Γ_c [marked by the transparent green plane in Figs. 1(b) and 1(c)] from a "deterministic" to a "random" scattered wave. Below Γ_c the scattered field is *chiral*, i.e., it consists of *only one* eigenmode of the instantaneous scattering matrix S^t, while its projection to the other basis vector is negligible. The specific eigenstate that represents the scattered field depends on the encircling handedness of the parametric loop around the EP. For example, in case of Fig. 1(b) where the parameters $[\epsilon(t), \kappa(t)]$ encircle the EP in a clockwise (CW) direction, the coefficient $\tilde{b}_2 \approx 0$ while $\tilde{b}_1$ remains on the unit circle irrespective of the specific features of the incident wave. When the encircling is counterclockwise (CCW), the coefficient $\tilde{b}_1 \approx 0$ while $\tilde{b}_2$ remains on a unit circle, see Fig. 1(c). Above Γ_c, the scattered field is, in general, a linear combination of both eigenvectors $\{|\mu_{1,2}^t\rangle\}$ with $\tilde{b}_n$ reflecting the dependence of the outgoing field on the specific properties of the incident waves.

The abrupt transition from a chiral fixed point attractor to a stochastic scattered signal is also evident from the analysis of the outgoing fields in the channel representation, i.e., $|S^-(t)\rangle = (S_1^-(t), S_2^-(t))^T$. In Figs. 2(a) and 2(b) we show the real and the imaginary part of the ratio between the left and right outgoing scattered fields S_2^-/S_1^- for two values of Γ, being above or below $\Gamma_c \equiv 1/\tau_c$. We also show the scattered field for a CW and a CCW encircling around the EP. The results reconfirm the conclusions drawn from the previous analysis using the

instantaneous scattering matrix basis, see Figs. 1(b) and 1(c). Namely, for $\Gamma < \Gamma_c$, the relative scattered right over left field amplitudes are insensitive to the characteristics of the incident wave [see Fig. 2(a)] and depend only on the handedness of the encirclement; for $\Gamma > \Gamma_c$ the relative scattered right over left amplitudes vary widely, becoming highly sensitive to the characteristics of the initial wave. We have confirmed via simulations that the scattered fields demonstrate the same features as the ones shown in Figs. 1(b), 1(c), 2(a), and 2(b) irrespective of the incident frequency ω in a broad frequency range $\omega \in [-2\gamma, 2\gamma]$. For loops far away from an EP, the scattered field appears to be again sensitive to the shape of the incident wave [50].

The existence of a chiral fixed-point attractor in the scattered field for $\Gamma < \Gamma_c$ is particularly intriguing. A heuristic explanation of its occurrence is given by considering the extreme case in which, during the parametric cycle, the field $|\Psi(t)\rangle$ inside the scatterer follows the instantaneous eigenstate of the effective Hamiltonian H^t_{eff} corresponding to an eigenvalue that has the largest imaginary part. The total amplification (or attenuation) experienced by such mode at the end of the evolution cycle is $I \approx \int_0^{2\pi/\Omega} \max[\text{Im}(\lambda^t_{\text{eff},1}, \lambda^t_{\text{eff},2})]dt$, and it splits in two contributions: one associated with the amplification or attenuation due to the evolution under $H_0(t)$ and one due to a pure attenuation mechanism attributed to the "escape" of the field to the continuum. These two competing mechanisms determine the magnitude of the internal field $|\Psi(t)\rangle$, see the first Eq. (4), which influences the formation of the scattered wave. The latter, according to Eq. (4b), consists of two terms: the leaking internal field and the incoming wave, corresponding to the second and first term in Eq. (4). If $I > 0$, the leaking internal field will dominate over the incident wave and it will determine the form of the scattered field. If, on the other hand, $I < 0$ (due to strong coupling to the continuum), the internal field will eventually subside and the waves $|S^+(t)\rangle$ will strongly influence the form of the scattered field $|S^-\rangle$.

The above argument assumes that the internal quasiadiabatic dynamics [50] is not affected by the presence of the radiative losses (due to coupling to the continuum) and the additive incoming fields $|S^+(t)\rangle$ [see the first Eq. (4)]. Indeed, we have analytically shown (see the Supplemental Material [50]) that this assumption is valid.

Electronic circuits.—We validated these predictions using an electronic circuit scattering setup. The circuit consists of two LC resonators (dimer), see Fig. 3, one being lossy due to the presence of a resistor R, while the other one experiencing a balanced amount of gain due to an amplifier $-R$. The inductances L at both resonators are equivalent. The capacitances at the left and right resonators are $C_1 = C(1-\epsilon)$ and $C_2 = C(1+\epsilon)$, respectively, where $\epsilon \ll 1$ is a time-modulated parameter. Each LC resonator ($\epsilon = 0, R \to \infty$) has a resonant angular

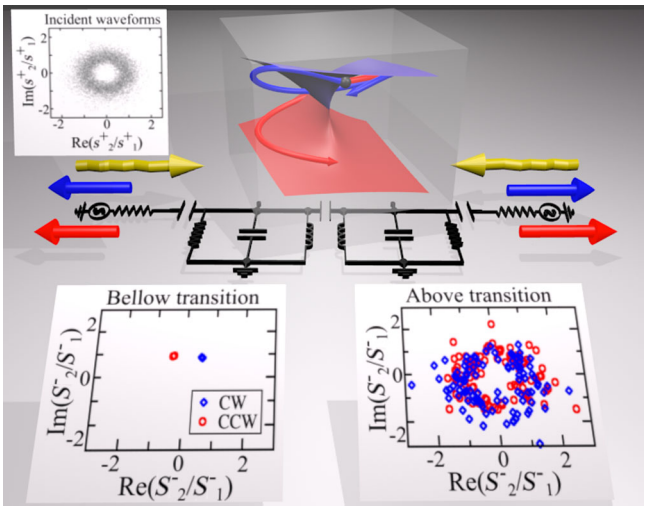

FIG. 3. Electric-circuit scattering setup where a quasiadiabatic encirclement of an EP degeneracy can lead to a chiral control of the scattered field when the coupling to TLs is smaller than a critical value. The outgoing scattered field, $|S^-_V\rangle = (S^-_1, S^-_2)^T$, has an attractor determined by the direction of encircling (bottom left). When the coupling to the continuum is large, the outgoing field is sensitive to the specific features of the incident field.

frequency $\omega_0 = 1/\sqrt{LC} = 2\pi$ GHz and resonant impedance $Z_0 = \sqrt{L/C} = 70$ Ohms. The two resonators are coupled via a capacitor $C_c = \kappa C$. The circuit is connected to transmission lines (TL), represented through their Thevenin equivalent, consisting of a grounded voltage source connected in series to the reference resistance $R_0 = 50$ Ohms and capacitively coupled through $C_e = \delta C$ to the nodes of the left and right resonators, V_1 and V_2, see Fig. 3.

Using Kirchoff's laws, we evaluated the parameters for which the isolated circuit ($C_e = 0$) has EP degeneracies [50]. The eigenfrequencies of this system are

$$\omega^2 = \frac{\pm\sqrt{(2\kappa-\gamma^2)^2 - 4\gamma^2} + 2(1+\kappa) - \gamma^2}{2(1+2\kappa)} \tag{7}$$

where $\omega = \tilde{\omega}/\omega_0$ and $\gamma \equiv Z_0/R$. Consequently, the EP occurs whenever the term inside the square root is zero, i.e., $\kappa = \gamma(1+\gamma/2)$. A quasiadiabatic loop around the EP is realized by a time-variation of the capacitances of each of the two LC resonators and of the coupling capacitance, i.e., $\epsilon(t) = \epsilon_0 \sin(\Omega t)$ and $\kappa = \kappa_0[1 + \ell \cos(\Omega t)]$, where $\Omega = 1$ MHz is the modulation frequency and $\epsilon_0 = 0.05$, $\ell = 0.3$, and $\kappa_0 = 0.105$.

The incident (monochromatic) voltages waves $|S^+_V(t)\rangle = (s^+_1, s^+_2)^T e^{i\tilde{\omega}t} = \frac{1}{2}(V^s_1, V^s_2)^T e^{i\tilde{\omega}t}$ are generated by driving the nodes V_L and V_R (see Fig. 3), with time dependent (Thevenin equivalent) voltage sources $v^s_{1,2}(t) = \mathcal{R}e(V^s_{1,2}e^{i\tilde{\omega}t})$. We have considered an ensemble of incident waves resulting from voltage sources with random amplitudes $V^s_{1(2)}$ and

phases [50]. The outgoing waves at the two transmission lines are written as $|S_V^-(t)\rangle = [S_1^-(t), S_2^-(t)]^T$, where $v_{1,2}^-(t) = \mathcal{R}e\{S_{1,2}^-(t)\}$. We have evaluated the outgoing voltages at multiples of the driving period and after a transient time of two-three driving periods [51]. Figure 3 shows that, for weak coupling to the transmission lines, the system reaches a fixed-point attractor which depends only on the direction of the loop encircling the EP. In contrast, when the coupling to the TL is strong, the outgoing signal demonstrates a sensitivity to the preparation of the incident wave, see Fig. 3.

Conclusions.—We have investigated the scattering from an adiabatically driven target which supports an EP degeneracy. We find that the scattered field is insensitive to the shape of the incident wave and the operational details of the driving. This occurs when the parametric path of the driving encircles the EP and the dwell time of the scattering process is above a critical value τ_c. The latter is associated with the inverse growth rate of the field inside the scattering target during one period of the adiabatic driving. Under these conditions, the scattered field approaches a fixed point. The sensitivity to the incident wave is abruptly regained when the dwell time becomes smaller than τ_c. We have tested the validity of these results in an electronic circuit. It will be interesting to test this robustness of the outgoing field against initial conditions in more challenging scattering scenarios where, for example, chaotic scattering prevails [52,53].

L. J. F.-A. and T. K. acknowledge partial support from ONR Grant No. N00014-16-1-2803 and from AFOSR Grant No. FA 9550-14-1-0037. F. E. acknowledges support from NSF Grant No. CMMI-1925543. A. A. and H. L. were supported by the Air Force Office of Scientific Research and by the Defense Advanced Research Project Agency.

[*] These authors contributed equally to the results of this Letter.

[1] U. Leonhardt, Optical conformal mapping, Science **312**, 1777 (2006).
[2] V. G. Veselago, The electrodynamics of substances with simultaneously negative values of ϵ and μ, Sov. Phys. Usp. **10**, 509 (1968).
[3] J. B. Pendry, Negative Refraction Makes a Perfect Lens, Phys. Rev. Lett. **85**, 3966 (2000).
[4] R. A. Shelby, D. R. Smith, and S. Schultz, Experimental verification of a negative index of refraction, Science **292**, 77 (2001).
[5] V. M. Shalaev, W. Cai, U. K. Chettiar, H. Yuan, A. K. Sarychev, V. P. Drachev, and A. V. Kildishev, Negative index of refraction in optical metamaterials, Opt. Lett. **30**, 3356 (2005).
[6] J. B. Pendry, D. Schurig, and D. R. Smith, Controlling electromagnetic fields, Science **312**, 1780 (2006).
[7] A. Alù and N. Engheta, Achieving transparency with plasmonic and metamaterial coatings, Phys. Rev. E **72**, 016623 (2005).
[8] D. L. Sounas, R. Fleury, and A. Alù, Unidirectional Cloaking Based on Metasurfaces with Balanced Loss and Gain, Phys. Rev. Applied **4**, 014005 (2015).
[9] F. Monticone and A. Alú, Do Cloaked Objects Really Scatter Less?, Phys. Rev. X **3**, 041005 (2013).
[10] D. Rainwater, A. Kerkhoff, K. Melin, J. C. Soric, G.Moreno, and A. Alù, Experimental verification of three-dimensional plasmonic cloaking in free-space, New J. Phys. **14**, 013054 (2012).
[11] Y. D. Chong, L. Ge, H. Cao, and A. D. Stone, Coherent Perfect Absorbers: Time-Reversed Lasers, Phys. Rev. Lett. **105**, 053901 (2010).
[12] W. Wan, Y. Chong, L. Ge, H. Noh, A. D. Stone, and H. Cao, Time-reversed lasing and interferometric control of absorption, Science **331**, 889 (2011).
[13] H. Li, S. Suwunnarat, R. Fleischmann, H. Schanz, and T. Kottos, Random Matrix Theory Approach to Chaotic Coherent Perfect Absorbers, Phys. Rev. Lett. **118**, 044101 (2017).
[14] S. Longhi, $\mathcal{PT}$-symmetric laser absorber, Phys. Rev. A **82**, 031801(R) (2010).
[15] Y. Sun, W. Tan, H. Q. Li, J. Li, and H. Chen, Experimental Demonstration of a Coherent Perfect Absorber with $\mathcal{PT}$ Phase Transition, Phys. Rev. Lett. **112**, 143903 (2014).
[16] D. G. Baranov, A. Krasnok, T. Shegai, A. Alu, and Y. Chong, Coherent perfect absorbers: Linear control of light with light, Nat. Rev. Mater. **2**, 17064 (2017).
[17] M. Davy and A. Z. Genack, Selectively exciting quasinormal modes in open disordered systems, Nat. Commun. **9**, 4714 (2018).
[18] I. M. Vellekoop and A. P. Mosk, Universal Optimal Transmission of Light Through Disordered Materials, Phys. Rev. Lett. **101**, 120601 (2008).
[19] K. G. Makris, R. El-Ganainy, D. N. Christodoulides, and Z. H. Musslimani, Beam Dynamics in $\mathcal{PT}$ Symmetric Optical Lattices, Phys. Rev. Lett. **100**, 103904 (2008).
[20] R. El-Ganainy, K. Makris, Z. H. Khajavikhan, S. Rotter, and D. N. Christodoulides, Non-Hermitian physics and $\mathcal{PT}$ symmetry, Nat. Phys. **14**, 11 (2018).
[21] L. Feng, R. El-Ganainy, and L. Ge, Non-Hermitian photonics based on parity-time symmetry, Nat. Photonics **11**, 752 (2017).
[22] S. K. Özdemir, S. Rotter, F. Nori, and L. Yang, Parity-time symmetry and exceptional points in photonics, Nat. Mater. **18**, 783 (2019).
[23] M.-A. Miri and A. Alu, Exceptional points in optics and photonics, Science **363**, eaar7709 (2019).
[24] Z. Lin, H. Ramezani, T. Eichelkraut, T. Kottos, H. Cao, and D. N. Christodoulides, Unidirectional Invisibility Induced by PT-Symmetric Periodic Structures Phys. Rev. Lett. **106**, 213901 (2011).
[25] R. Fleury, D. Sounas, and A. Alú, An invisible acoustic sensor based on parity-time symmetry, Nat. Commun. **6**, 5905 (2015).
[26] L. Feng, Y.-L. Xu, W. S. Fegadolli, M.-H. Lu, J. E. B. Oliveira, V. R. Almeida, Y.-F. Chen, and A. Scherer, Experimental demonstration of a unidirectional reflectionless

parity-time metamaterial at optical frequencies, Nat. Mater. **12**, 108 (2013).
[27] H. Ramezani, T. Kottos, R. El-Ganainy, and D. N. Christodoulides, Unidirectional nonlinear $\mathcal{PT}$-symmetric optical structures, Phys. Rev. A **82**, 043803 (2010).
[28] N. Bender, S. Factor, J. D. Bodyfelt, H. Ramezani, D. N. Christodoulides, F. M. Ellis, and T. Kottos, Observation of Asymmetric Transport in Structures with Active Nonlinearities, Phys. Rev. Lett. **110**, 234101 (2013).
[29] B. Peng, S. K. Özdemir, F. Lei, F. Monifi, M. Gianfreda, L. G. Long, S. Fan, F. Nori, C. M. Bender, and L. Yang, Parity-time-symmetric whispering-gallery microcavities, Nat. Phys. **10**, 394 (2014).
[30] L. Chang, X Jiang, S. Hua, C. Yang, J. Wen, L. Jiang, G. Li, G. Wang, and M. Xiao, Parity-time symmetry and variable optical isolation in active-passive-coupled microresonators, Nat. Photonics **8**, 524 (2014).
[31] H. Hodaei, M.-A. Miri, M. Heinrich, D. N. Christodoulides, and M. Khajavikhan, Parity-time-symmetric microring lasers, Science **346**, 975 (2014).
[32] L. Feng, Z. J. Wong, R.-M. Ma, Y. Wang, and X. Zhang, Single-mode laser by parity-time symmetry breaking, Science **346**, 972 (2014).
[33] H. Xu, D. Mason, L. Jiang, and J. G. E. Harris, Topological dynamics in an optomechanical system with highly non-degenerate modes, arXiv:1703.07374.
[34] J. Doppler, A. A. Mailybaev, J. Böhm, U. Kuhl, A. Girschik, F. Libisch, T. J. Milburn, P. Rabl, N. Moiseyev, and S. Rotter, Dynamically encircling an exceptional point for asymmetric mode switching, Nature (London) **537**, 76 (2016).
[35] H. Xu, D. Mason, L. Jiang, and J. G. E. Harris, Topological energy transfer in an optomechanical system with exceptional points, Nature (London) **537**, 80 (2016).
[36] Q. Zhong, M. Khajavikhan, D. N. Christodoulides, and R. El-Ganainy, Winding around non-Hermitian singularities, Nat. Commun. **9**, 4808 (2018).
[37] R. Uzdin, A. Mailybaev, and N. Moiseyev, On the observability and asymmetry of adiabatic state flips generated by exceptional points, J. Phys. A **44**, 435302 (2011).
[38] T. T. Koutserimpas, A. Alú, and R. Fleury, Parametric amplification and bidirectional invisibility in PT-symmetric time-Floquet systems, Phys. Rev. A **97**, 013839 (2018).
[39] D. Halpern, H. Li, and T. Kottos, Floquet protocols of adiabatic state flips and reallocation of exceptional points, Phys. Rev. A **97**, 042119 (2018).
[40] S. Suwunnarat, D. Halpern, H. Li, B. Shapiro, and T. Kottos, Dynamically modulated perfect absorbers, Phys. Rev. A **99**, 013834 (2019).
[41] H. Li, A. Mekawy, and A. Alù, Beyond Chu's Limit with Floquet Impedance Matching, Phys. Rev. Lett. **123**, 164102 (2019).
[42] T. Gao, E. Estrecho, K. Y. Bliokh, T. C. H. Liew, M. D. Fraser, S. Brodbeck, M. Kamp, C. Schneider, S. Höfling, Y. Yamamoto, F. Nori, Y. S. Kivshar, A. G. Truscott, R. G. Dall, and E. A. Ostrovskaya, Observation of non-Hermitian degeneracies in a chaotic exciton-polariton billiard, Nature (London) **526**, 554 (2015).
[43] P. Peng, W. Cao, C. Shen, W. Qu, J. Wen, L. Jiang, and Y. Xiao, Anti-parity-time symmetry with flying atoms, Nat. Phys. **12**, 1139 (2016).
[44] Z. Zhang, Y. Zhang, J. Sheng, L. Yang, M. A. Miri, D. N. Christodoulides, B. He, Y. Zhang, and M. Xiao, Observation of Parity-Time Symmetry in Optically Induced Atomic Lattices, Phys. Rev. Lett. **117**, 123601 (2016).
[45] H. Jing, S. K. Özdemir, X. Y. Lu, J. Zhang, L. Yang, and F. Nori, $\mathcal{PT}$-Symmetric Phonon Laser, Phys. Rev. Lett. **113**, 053604 (2014).
[46] J. Zhang, B. Peng, S. K. Özdemir, K. Pichler, D. O. Krimler, G. Zhao, F. Nori, Y.-X. Liu, S. Rotter, and L. Yang, A phonon laser operating at an exceptional point, Nat. Photonics **12**, 479 (2018).
[47] X. Zhu, H. Ramezani, C. Shi, J. Zhu, and X. Zhang, $\mathcal{PT}$-Symmetric Acoustics, Phys. Rev. X **4**, 031042 (2014).
[48] H. Li, M. Chitsazi, R. Thomas, F. M. Ellis, and T. Kottos, $\mathcal{PT}$-symmetry and non-Hermitian wave transport in microwaves and RF circuits, in *Parity-Time Symmetry and Its Applications*, Springer Tracts in Modern Physics Vol. 280, edited by D. Christodoulides and J. Yang (Springer, Singapore, 2018).
[49] In fact, ω is the frequency detuning with respect to a reference frequency associated with the resonant frequency of the resonators (modes) at $t = 0$.
[50] See the Supplemental Material at http://link.aps.org/supplemental/10.1103/PhysRevLett.124.133905 for further details on (A) the performance of the operation away from the EP, (B) a theoretical understanding of a scattering-field-control transition near the EP, and (C) electronic circuit simulations.
[51] Circuit simulations were performed using NGSpice V. 28plus, http://ngspice.sourceforge.net/.
[52] T. Kottos and H. Schanz, Quantum graphs: A model for quantum chaos, Physica (Amsterdam) **9E**, 523 (2001).
[53] T. Kottos and U. Smilansky, Chaotic Scattering on Graphs, Phys. Rev. Lett. **85**, 968 (2000).